

www.acsanm.org Article

# Charge-Inhomogeneity-Mediated Low-Frequency Noise in One-Dimensional Edge-Contacted Graphene Heterostructure Field Effect Transistors

Aroop K. Behera, C. Thomas Harris, Douglas V. Pete, Christopher M. Smyth, Marta B. Muniz, Ozhan Koybasi, Takashi Taniguchi, Kenji Watanabe, Branson D. Belle, and Suprem R. Das\*



Cite This: ACS Appl. Nano Mater. 2024, 7, 12366-12375



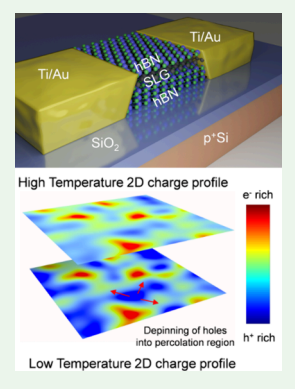
**ACCESS** 

III Metrics & More

Article Recommendations

s Supporting Information

ABSTRACT: We have previously shown that one-dimensional edge contact to two-dimensional heterostructure field effect transistors with a graphene channel, and hexagonal boron nitride, as both the substrate material and top encapsulated layer, show ultrahigh carrier mobility and ultralow carrier noise (low frequency noise, LFN). Although the noise mechanism of the transistor devices in the ON state was modeled based on microscopic scattering mechanisms caused by charge carriers and phonons, the model was based on normalized noise spectral density following Hooge's noise model in the ON-state. In this article, we show that the normalized noise current densities within the charge residual region of two similarly fabricated edge-contacted and encapsulated graphene heterostructure field effect transistors show different trends with overdrive voltage that resemble previously reported results in the literature. Here we explain the poorly understood and conflicting LFN trends in the charge residual region (low charge carrier regime) by correlating the spatial charge inhomogeneity near the Dirac point in heterostructure devices to electron—hole puddles. By systematically studying the temperature-dependent transport, LFN and by modeling the channel characteristics in such devices within the charge



residual region, we show that the carriers inside electron—hole puddles get pinned at lower temperatures and unpinned at higher temperatures, as consistently shown in their normalized flat-band spectral variation as a function of overdrive voltage. More generally, near the charge neutrality region of single-layer graphene devices, the LFN is described by a correlated carrier number and mobility fluctuations of the charge carriers. Understanding the carrier physics in encapsulated high-performance and edge-contacted heterostructure two-dimensional devices will aid us in not only engineering low-noise graphene-based FETs for future digital and analog electronics but also understanding the noise associated with Dirac-type materials.

**KEYWORDS:** Electron—hole puddles, Encapsulated graphene, Hexagonal boron nitride, Low-frequency noise, Heterostructure 2D field effect transistors

## ■ INTRODUCTION

Transport in monolayer graphene devices, mostly in field effect transistor (FET) configurations, has brought several fascinating discoveries, such as universal conductance fluctuation, weak localization, phase coherence, and half integer quantum Hall effect, to name a few. 1-4 For practical applications, graphene has also been used as a model two-dimensional atomically thin material system due to its exceptionally high electronic mobility, thermal conductivity, mechanical stiffness, and optical transparency, almost all of which have been linked to its linear band dispersion and associated massless Dirac fermions. 5-11 Due to its outstanding transport properties, it has also been shown that the charge carriers in a graphene FET (GFET) are sensitive enough (especially near the charge neutrality point or Dirac point) to differentiate the current fluctuations from those of their conventional counterparts such as a silicon FET. 12 Such fluctuations were also ascribed to monolayer graphene's linear band structure. However, unexpected charge carrier screening (leading to an inverse

noise amplitude trend) has also been observed in a bilayer GFET. Subsequently, a number of reports have studied the scattering mechanisms experienced in GFETs fabricated on SiO<sub>2</sub> dielectrics to demonstrate the effects of charge impurities and interface states in the oxide as well as at the oxide—graphene interface, respectively. The findings have been corroborated with noise studied in GFETs with suspended channels. Low-frequency noise (LFN) is important to understand and control in FET devices from several practical standpoints, including but not limited to RF applications and precision biosensing. Due to their ultrahigh mobility, ballistic transport when encapsulated by hexagonal boron nitride

Received: January 18, 2024
Revised: April 21, 2024
Accepted: May 7, 2024
Published: May 16, 2024





(hBN), and linear ON current scaling with applied overdrive voltage, GFETs have been proposed as future candidates for RF wireless communication. <sup>18–21</sup> Moreover, GFETs have also been attributed with shifting Dirac points as a method for sensing different biomolecules (e.g., glucose, immunoglobulin, etc.) and living cell activities (e.g., *E. coli* in solution). <sup>22–25</sup> Therefore, it is important to develop high-performance GFET devices and understand their LFN characteristics at the charge neutrality point (CNP) or the Dirac point.

In a transistor device the resistance fluctuation model, explained by carrier mobility fluctuations in the device channel, is termed as Hooge's model with the noise in the system characterized by a dimensionless quantity called Hooge's parameter.<sup>26</sup> On the other hand, a second model relying on the number density fluctuation of the charge carriers in the semiconducting channel by random trapping and detrapping of free carriers by traps in the substrate with time constant distributions is explained by McWhorter's model.<sup>27</sup> Many LFN studies have recently been performed on graphene FETs (GFETs), and both fluctuation models have been employed in data analysis. 14,16,28-30 While the ON state noise in GFETs has been extensively studied, understanding charge carrier dynamics and the consequent 1/f noise, especially in the charge residual region, will shed light on properties of electron-hole puddles. A few studies have been performed, explicitly addressing the 1/f noise characteristics in the charge residual region of graphene. 15,31,32 Xu et al. first addressed the effect of space-charge inhomogeneity on 1/f noise near the Dirac point of GFETs using Hooge's model and analyzed the change in puddle size with applied gate voltage to explain their observation in GFETs fabricated on SiO<sub>2</sub> substrate.<sup>31</sup> Takeshita et al. attributed the anomalous behavior of noise in GFETs at the Dirac point with pinning and depinning of puddles in the channel.<sup>32</sup> Kumar et al. have studied the behavior of noise in hBN-encapsulated GFETs and have explained the total noise observed around the CNP as noise contributions from the contacts and channel. 15 Although a few studies have been performed on GFETs supported and encapsulated by hBN, understanding the role of electronhole puddles in observed low-frequency noise around the charge neutrality point as a function of operating temperature in such heterostructure GFETs has not been addressed. 15,33-36

Subsequent developments in GFETs have achieved substantial milestones: first, the introduction of hexagonal boron nitride (hBN) as dielectric substrates as well as a top encapsulation layer to two-dimensional (2D) channels in the GFETs, and second, the ability to form one-dimensional (1D) edge-contacts to 2D heterostructure GFETs (2D-HGFETs). 17,37-40 Due to close lattice matching between graphene and hBN, the near-epitaxial interface provides very high carrier mobility while reducing the carrier scattering substantially. As such, combining the above two device architectures, 1-D edge contacts to 2D-HGFETs with hBN lead to outstanding transport properties. 20,21,41,42 Although at low temperatures (~4 K) ballistic transport has been demonstrated in these edge-contacted devices, in our previous study we have demonstrated their ultralow noise properties with Hooge parameters of  $\sim 10^{-5}$  at 80 K and  $\sim 10^{-3}$  at 300 K. However, the latter study was conducted at the ON state of a single-layer graphene (SLG) device following the mobility fluctuation model, where the carrier concentration is high. Microscopic origins of the noise arising from several scattering events, such as short-range scattering, long-range

Coulombic scattering, longitudinal acoustic (LA) phonon scattering, and remote interfacial phonon (RIP) scattering, were shown to be associated with the obtained noise. Although the model was extended to within the charge residual region around the Dirac point in the SLG device, there are number of studies that have shown that the carrier concentration at the Dirac point is orders of magnitude smaller than that at its ON state and the spatial charge distribution forms electron-hole puddles. Models have also been developed to understand the electronic transport in this regime and confirm a percolation transport physics in this region. 5,44-49 Some prior studies on LFN in the Dirac region have been made where they have used either Hooge's noise model (a mobility fluctuation model that is usually valid at a high carrier concentration regime) or microscopic scattering models based on various scattering mechanisms. Consequently, several conflicting noise trends (such as V-shaped vs  $\Lambda$ -shaped) have been reported in the literature at the charge neutrality region. Takeshita et al. have recently attributed the anomalous behavior of noise in GFETs at the Dirac point to the pinning and depinning of puddles in the channel but without any explanation of the detailed underlying physics. The low charge carrier concentrations as well as percolation transport channel arising from electronhole puddle physics, therefore, should provide fundamentally different noise mechanisms in these devices in the charge neutrality region (characterized by the McWorter model).

In this work, we systematically study the temperature-dependent electrical transport and 1/f LFN on 1D contacts to 2D-HGFET and attribute specifically the role of electron—hole puddles contributing to the flat band fluctuation model in two identical devices to elucidate noise characteristics at the CNP.

#### DEVICE FABRICATION AND EXPERIMENT

Two SLG 2D-HGFETs with 1D edge contacts were fabricated using an hBN/SLG/hBN heterostructure by a viscoelastic dry stamping method, <sup>50</sup> as shown in Figure 1a. For convenience, we label the devices as "device 1" and "device 2", respectively. The heterostructures consisted of a bottom hBN flake of thickness ~50 nm, an SLG channel, and a top encapsulated hBN of thickness ~20 nm. Electron-beam lithography and reactive ion etching techniques were used to make one-dimensional edge contacts with 5 nm Ti and 80 nm

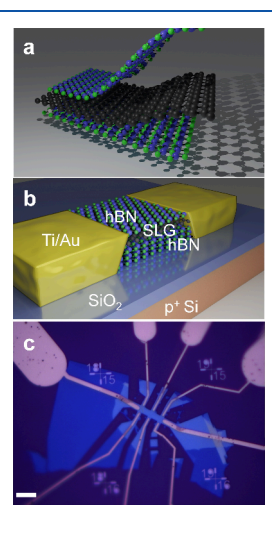


Figure 1. (a) Schematic showing viscoelastic stamping of bottom hBN, SLG, and top hBN. (b) Schematic showing an edge-contacted heterostructure field effect transistor. (c) Micrograph of a fabricated 2D-HGFET with SLG as the transistor channel (scale bar: 5  $\mu$ m).

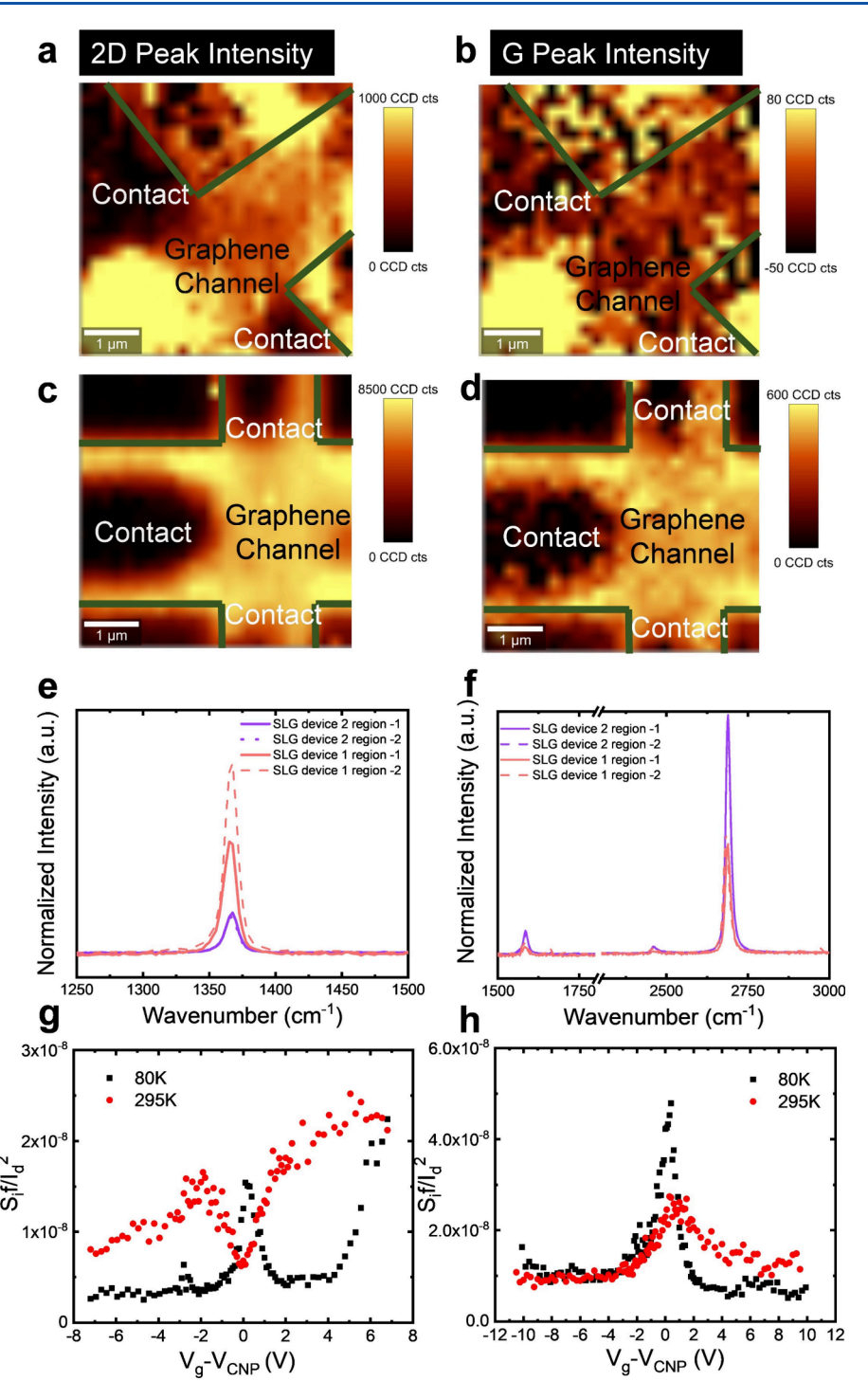


Figure 2. (a, b) Raman maps of graphene 2D and G mode integrated peak intensities detected from device 1. (c, d) Raman maps of graphene 2D and G mode integrated peak intensities detected from device 2. The scale bars in (a–d) represent 1  $\mu$ m. (e, f) Raman spectra collected from the channel regions of devices 1 and 2 showing hBN and graphene peaks, respectively, and (g, h) LFN characteristics of devices 1 and 2, respectively, showing normalized noise spectral density.

Au for source-drain contacts. <sup>20</sup> A heavily doped (p-type) Si substrate was used as the global back gate. The fabricated devices have 9 and 6  $\mu$ m channel lengths, respectively, and 2  $\mu$ m of channel width. A schematic of the edge contacted device is shown in Figure 1b with an optical image of the device shown in Figure 1c. We performed temperature-dependent transport and noise studies from 80 to 295 K. All the required voltages for three terminal measurements were supplied via Keithley 2400 SMUs accompanied by low-pass RC filters to cut off any spurious noise originating from SMUs. The source-drain current was amplified by using a Model DL-1211 transimpedance

amplifier and fed into an HP 34401 digital multimeter to read the drain current values. The voltage output from the preamplifier was also fed to an HP-3588A spectrum analyzer to record the power spectral density to characterize device noise.

To verify the quality of the hBN/SLG/hBN heterostructures, the interface cleanliness and graphene layer number were probed after device fabrication by using Raman spectroscopy. Point spectroscopic measurements and Raman mapping were conducted by using a WITec Raman spectrometer. A 532 nm laser source was used with a 100× objective and 200  $\mu\rm W$  power. Spectra were acquired using a 25

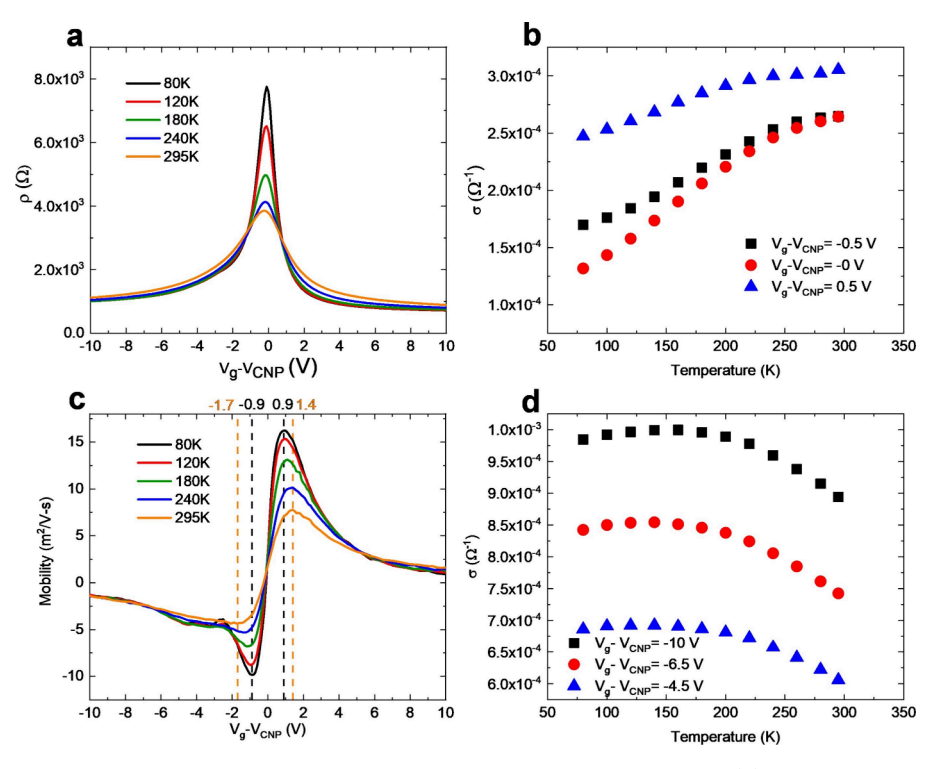


Figure 3. (a) Measured resistance as a function of  $V_{\rm g}-V_{\rm CNP}$  at different operating temperatures. (b) Extracted conductivity as a function of operating temperature at three different  $V_{\rm g}-V_{\rm CNP}$  in the residual region. (c) Extracted field effect mobility as a function of  $V_{\rm g}-V_{\rm CNP}$  at different operating temperatures. (d) Extracted conductivity as a function of operating temperature at three different  $V_{\rm g}-V_{\rm CNP}$  away from the charge residual region.

s acquisition time per point, and maps were obtained using a  $25 \times 25$  point grid with 200 nm step size.

# ■ RESULTS AND DISCUSSION

Figure 1 shows a schematic diagram of hBN/SLG/hBN heterostructure stacks that were used to fabricate devices 1 and 2. Figure 1b shows a schematic representation of the 1D edge contacts to the 2D heterostructure on a silicon chip with a heavily p-doped body and a 300 nm thermally grown oxide. The detailed fabrication procedure is described in our previous report. 43 Figure 1c shows the optical image (top view) of a representative fabricated 2D-HGFET device. Devices 1 and 2 studied in this report share similar fabrication processes, device configurations, and bottom hBN thicknesses (~50 nm). However, we note a variation in their top hBN encapsulating layer thickness: device 1 has an ~50 nm top hBN encapsulant and device 2 has an  $\sim$ 10 nm top hBN encapsulant. Figure 2a,b shows Raman maps obtained from device 1, while Figure 2 c,d shows Raman maps obtained from device 2. The color scale in Figure 2a,c represents the 2D mode peak integrated intensity, while the color scale in Figure 2b,d represents the integrated intensity of the G mode peak in the vicinity of each GFET channel. Both devices show the graphene peaks in the channel area (note that the graphene channel and the metal contact area have been labeled). While clear 2D and G mapping signals of the channel in device 2 are evident, the integrated intensities of the 2D and G modes are relatively weak in device 1, which we attribute to a thicker hBN encapsulation layer of the corresponding heterostructure stack. To verify that monolayer graphene is present in both devices, two regions in the mapped areas of each of the devices were chosen for spectral analysis. Figure 2 e,f shows the Raman spectra collected in the wavenumber ranges of the hBN peak and graphene (2D, G)

peaks, respectively. The spectra clearly show the high-quality material stack with the principal hBN peak (E<sub>2g</sub> peak) and graphene G peak and 2D peak. Throughout the mapped regions, the 2D peak intensity is  $\sim 8 \times$  higher than the G peak intensity, which is a signature of SLG. The hBN mode intensity detected in device 2 is smaller than that of device 1, while all graphene mode peak intensities are higher in device 2 than in device 1, which indicates a thinner hBN encapsulation is present in device 2.51 Owing to the similarity of the two devices, one expects their qualitative LFN behavior to resemble each other. However, following our previously modeled LFN analysis in transistor ON state when its noise was measured and extended to the charge neutrality point/Dirac point, as shown in Figure 2g,h, they behave quite differently. 43 Device 1 also shows a reverse trend measured at 80 and 295 K. This variation in LFN is widely reported in the literature as well; however, a unified understanding of the mechanism of the LFN at the Dirac point (characterized by a charge residual region) is yet to be made. The goal of the present paper is to establish such an LFN theory to demonstrate the noise resemblance of the two analogous devices shown here. We will revisit this in the following section.

Figure 3 shows the transport measurement results from device 2 (the measurement results showing similar trends from device 1 have been reported earlier  $^{43}$  and will further be discussed here as needed). Figure 3a shows the measured resistivity  $(\rho)$  as a function of applied gate voltage with an offset from the charge neutrality point  $(V_{\rm g}-V_{\rm CNP})$  for a 2D-HGFET. The resistivity peak appearing at the Dirac point shows the minimal conductivity, and the resistivity gradually decreases as the gate voltage is increased to positive (negative) values, confirming electron (hole) types in the conduction (valence) band. Away from the Dirac point, we observe metal-

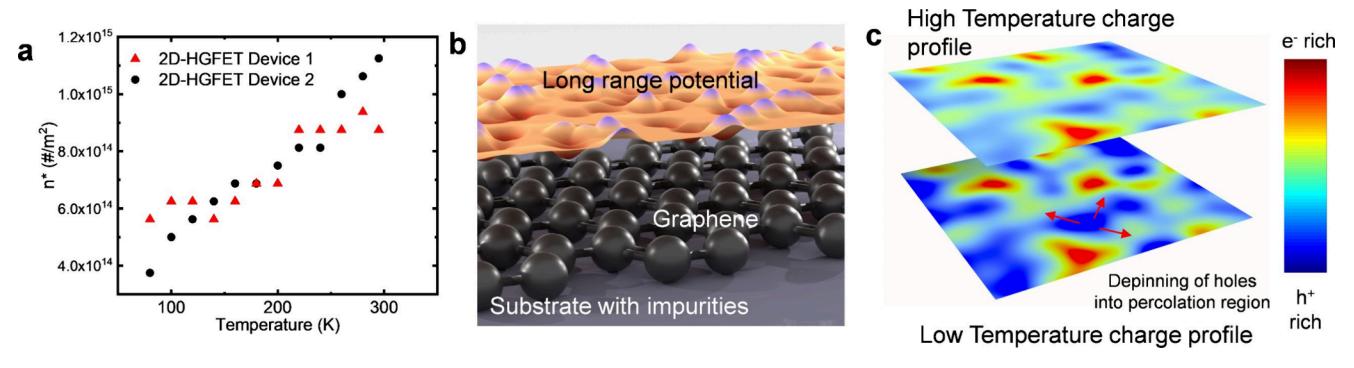


Figure 4. (a) Temperature variation of extracted rms charge concentration  $(n^*)$  in the percolation region of 2D-HGFET, (b) schematic model of long-range Coulombic potential arising from the charge impurities in the substrate, and (c) phenomenological model showing pinning and depinning of charge carriers into the percolation region and their temperature variation.

like behavior with conductivity increasing with decreasing temperature (see Figure 3d) and a nonmetallic behavior near the Dirac point where the conductivity decreases with decrease in temperature (see Figure 3b).<sup>43</sup>

First, to differentiate the region between metallic and nonmetallic behavior, we extracted the field effect mobility of the devices. The field effect mobility of the device is given by

$$\mu_{\rm FE} = \frac{g_{\rm m}}{C_{\rm ox} \times V_{\rm ds}} \frac{L}{W} \tag{1}$$

where  $g_{\rm m}$  is the transconductance given by  $(dI_{\rm ds}/dV_{\rm g})$ , L and Ware the channel length and width, respectively,  $V_{\rm ds}$  is the applied drain-source voltage, and  $C_{\rm ox}$  is the gate capacitance per unit area given by  $\varepsilon_{\rm ox}/d_{\rm ox}$ . Here  $\varepsilon_{\rm ox}$  is the gate dielectric constant  $(3 \times 10^{-11} \ {\rm F/m})$  and  $d_{\rm ox}$  is the gate dielectric thickness (300 nm). Global back gates for both fabricated devices were set that include an SiO2 dielectric below the bottom hBN layer (an actual dielectric constant of  $9.7 \times 10^{-5}$ is approximated as  $1 \times 10^{-4}$  F/m<sup>2</sup>). Figure 3c shows the extracted mobility for device 2, plotted as a function of  $V_{\sigma}$  - $V_{\rm CNP}$ . Mobility values of ~70,000 cm<sup>2</sup>/(V s) were obtained at 295 K and  $\sim$ 160,000 cm<sup>2</sup>/(V s) at 80 K. The mobility peaks for both electrons and holes are clearly seen at respective sides of the Dirac point with a sharp decrease in their values as the absolute value of the overdrive voltage increases. The orange and black dashed lines in Figure 3c are the reference overdrive voltages for mobility peaks obtained from the device at 295 and 80 K, respectively. The corresponding peak voltages for the device were 0.9 and 1.4 V at 80 and 295 K, respectively. We quantitatively differentiate the metallic and nonmetallic regime by defining a charge residual region as follows. The  $V_{\sigma}$ -  $V_{\rm CNP}$  values bound by the dashed lines for a given temperature on either side of the Dirac point are the charge residual region. It is important to note here that the width of the charge residual region is a function of temperature, where the width grows as the temperature increases.

Unlike a standard semiconducting channel where the carrier concentration is a direct function of overdrive gate voltage, here in graphene's charge residual region, the average channel carrier density is a constant value irrespective of gate bias, bound by the charge density induced by the voltage at mobility peak and is termed as  $n^*$ . With the increasing width of the charge residual region with temperature,  $n^*$  increases in value. It is in this residual region that the spatial profile of the graphene channel carries inhomogeneous puddles of electrons and holes, and the channel conductivity is governed by their

percolation transport.<sup>52</sup> The origin of the electron-hole puddles in the graphene channel has been attributed to Coulomb potentials arising from the charge impurities in the underlying substrate and to spatial modulation of the channel from ripples and bending. 53,54 Although hBN lacks charge impurities as compared to thermally grown SiO2 and provides an atomically flat surface for graphene to prevent folding, it has been shown that electron-hole puddles still exist in the graphene channel when hBN is used as a dielectric substrate. 55,56 To confirm the existence of electron-hole puddles in our channel, we plotted the extracted conductivity  $(\sigma = 1/\rho)$  as a function of the temperature. Figure 3b shows the conductivity of device 2 at different gate voltages within the charge residual region. Figure 3d, on the other hand, shows the device conductivity at different gate voltages away from the charge residual region. One can clearly observe the opposite trends shown by the conductivity with temperature in the residual and saturated regions. Such behavior in the conductivity within the charge residual region, the region of interest in this report, has been attributed to the presence of electron-hole puddles, 52,53 where the conductivity is described

$$\sigma(V_{g}) \approx \begin{cases} C \frac{e^{2}}{h} \frac{n(V_{g})}{n_{i}} & \text{for } n > n^{*} \\ C \frac{e^{2}}{h} \frac{n^{*}(T)}{n_{i}} & \text{for } n < n^{*} \end{cases}$$
(2)

where e is the fundamental electronic charge, h is Planck's constant, n is the carrier density related to gate voltage as n = n $C_{ox}V_{g}/e$ ,  $n^{*}$  is the residual carrier density (root-mean-square charge carrier density) in the percolation region considering the electron-hole puddle region induced by the substrate charge impurities of density  $n_i$ , C is a dimensionless parameter describing the strength of scattering, and T is the absolute temperature. As expected, the overall conductivity is minimum at the gate voltage corresponding to the CNP while the conductivity rises when the gate voltage moves away from the CNP. The increase in conductivity with temperature for the device for a given gate voltage (Figure 3b) in the residual region can be explained with the increasing value of  $n^*$  as the temperature rises, thus confirming the existence of puddles in the 2D-HGFET. The extracted values of  $n^*$  as a function of temperature is shown in Figure 4a, which clearly demonstrates a trend similar to that of the conductivity as a function of temperature, thus confirming the e-h puddle transport within

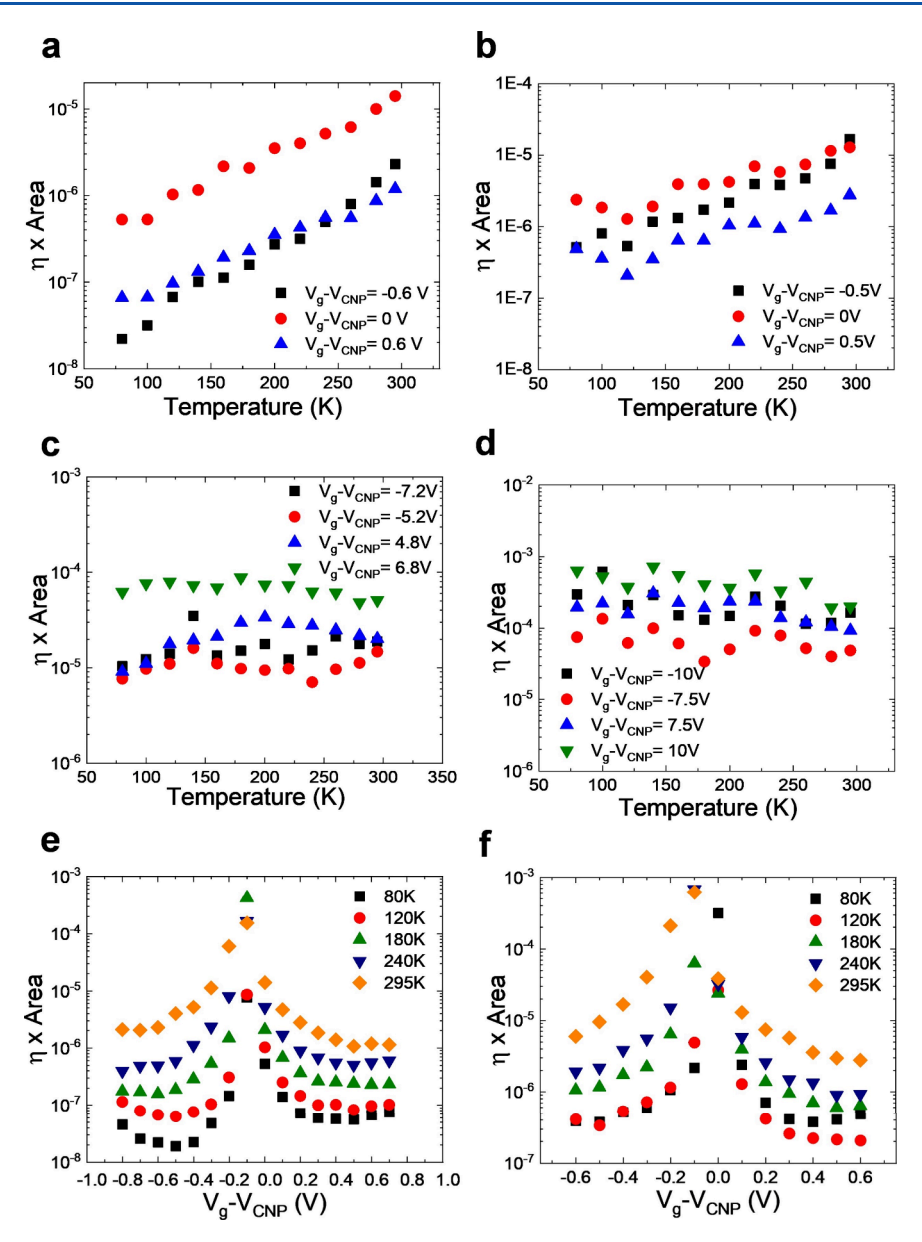


Figure 5. Area normalized flat band spectra as a function of operating temperature in the charge residual region for SLG device 1 (a) and SLG device 2 (b). Area normalized flat band spectra as a function of temperature away from charge residual spectra for SLG device 1 (c) and SLG device 2 (d). Area normalized flat band spectra as a function of overdrive gate voltage near CNP for the SLG device 1 (e) and SLG device 2 (f).

the charge residual region. This means at higher temperatures carriers in puddles gain enough thermal energy to escape into the conducting percolation region to participate in the electrical conduction. Figure 4b shows the schematic diagram of long-range Coulombic potential induced in the channel by the charge impurities  $(n_i)$  present in the substrate. This Coulombic potential gives rise to e-h puddles and a percolation region in the graphene channel, a phenomenological model qualitative schematic of which is provided in Figure 4c.

On the other hand, the behavior of conductivity away from the charge residual region, governed by diffusive transport with different scattering mechanisms, has previously been explained. The conductivity in the noncharge residual region shows a different trend (Figure 3d). As expected, with higher overdrive voltages, the conductivity increases as carrier density (n) in the channel increases. The decrease in conductivity with increasing temperature can be explained by considering

semiclassical diffusive conductivity model for the charge carriers

$$\sigma(T) = \frac{g_s g_v e^2 E_F \tau}{4\pi \hbar^2} \tag{3}$$

where  $g_s = g_v = 2$  are the spin and valley degeneracy factors, respectively,  $E_{\rm F}$  is the Fermi energy, and  $\tau$  is the scattering time given by  $\tau = \frac{\mu m^*}{e}$ . Here,  $\mu$  is carrier mobility and  $m^*$  is the effective carrier mass. The increase in temperature increases the average scattering events as the temperature rises, leading to a decrease in  $\tau$  and thus a decrease in conductivity. The microscopic origin and contributions to scattering from various scattering types in the ON state of the device (away from the charge residual region) in the encapsulated GFET has been extensively studied in our previous report. <sup>43</sup>

To understand the role of e-h puddles on electrical noise in 2D-HGFETs with 1-D contacts, specifically within the charge residual region of the two devices (devices 1 and 2, whose normalized noise current densities based on purely electronic diffusive transport look widely different, as shown in Figure 2g,h), we measured LFN by recording the normalized power spectral density in the devices in a frequency range from 2 Hz to 1.25 kHz. The average channel noise amplitude (A) normalized by area over all measured frequencies can be written as

$$A = \frac{1}{Z} \sum_{i=1}^{Z} f_i^{\gamma} (S_i / I_d^2)_i \times \text{area}$$
 (4)

where  $f_i$  is the frequency of measurement,  $\gamma$  is the exponent factor which generally lies between -0.8 and -1.2,  $S_i$  is the measured current power spectral density,  $I_d$  is the source-drain current. In this paper, we only analyze the noise results in the charge residual region in both of our devices. e-h puddles on substrates have been classified into two types, namely Type-I and Type-II, which are attributed to a small size with a relatively high carrier concentration and a large size with a relatively low carrier concentration, respectively.<sup>44</sup> It is important to emphasize that these Type-II puddles form the conducting path throughout the length of the graphene channel to facilitate carrier conduction, thereby giving rise to measurable current values, and are also termed as the "percolation region". 57 While previous studies on noise arising from e-h puddles on GFETs fabricated on SiO<sub>2</sub> dielectrics used the mobility fluctuation model to explain the V shape trend near the Dirac point and attributed it to the gradual increase and decrease in the size of Type-II puddles (with applied gate bias) as the reason for V shape, 31 however, Hooge's mobility fluctuation model is valid for homogeneous electrical channels with a single type of charge carriers with constant carrier concentration in the channel.<sup>26,58</sup> On the contrary, in our case here involving a percolation region, the number of carriers in the percolative network channels constantly changes. Therefore, using McWhorter's number fluctuation model within the charge neutrality region is more appropriate.<sup>2</sup>

Since in a MOS device the change in gate oxide charge density is equivalent to flat band voltage fluctuations, thus by using McWhorter's carrier number fluctuation model (encompassing, in our case, the dynamic charge trapping and detrapping from hBN surface to the percolative network channel via the e-h puddles), the measured current noise spectrum in our 2D-HGFETs can be described as<sup>59</sup>

$$\frac{S_I(f)}{I_{\rm d}^2} = \frac{g_{\rm m}^2}{I_{\rm d}^2} S_{V_{\rm fb}} \tag{5}$$

where  $S_{V_{\rm fb}}$  is the flat band voltage spectral density associated with charge fluctuations at the interface between the channel and the dielectric.  $S_{V_{\rm fb}}$  has been shown to be equal to the equivalent input gate voltage spectral density  $S_{V_{\rm g}}$ , where  $S_{V_{\rm fb}}$  is given as  $^{28,59,60}$ 

$$S_{V_{\text{fb}}} = \frac{6.2e^2k_{\rm B}T}{AfC_{\rm ox}^2k}D_{it} \tag{6}$$

where  $k_B$ , T, A, k, and  $D_{it}$  are Boltzmann's constant, temperature (in kelvin), channel area, inverse of decay scale in trap states  $\sim 10^9$  m<sup>-1</sup>, and trap density of hBN, respectively.

To better elucidate the dynamic trapping of charge carriers from the charge inhomogeneous graphene channel, we define a parameter  $\eta$  from our measured current noise spectrum, defined as<sup>28</sup>

$$\eta = \frac{S_l(f)}{I_d^2} \times \frac{I_d^2}{g_m^2} \times f \tag{7}$$

where f is the selected frequency for analysis, which was set to 100 Hz in our case. The physical significance of  $\eta$  could be understood as the rate of trapping and detrapping of charge carriers between the percolation region in the channel and the interface trap states in the dielectrics. This  $\eta$  is the factor that we define here as our device noise that we are going to further interpret below as the device is operated.

Figure 5a,b shows the behavior of  $\eta$  normalized by gate voltage and device area as a function of temperature for different overdrive voltages in the charge residual region for the two devices. On the other hand, Figure 5c,d shows the normalized  $\eta$  as a function of temperature for the same devices at overdrive voltages away from the charge residual region. The temperature dependence of flat band fluctuation in the charge residual region corresponds to the trapping and detrapping of carriers in the percolation region as shown previously in Figure 4c. The temperature independence of flat band fluctuation away from the charge residual region, on the other hand, indicates that the noise primarily arises from dynamic scattering mechanisms via mobility fluctuations.  $^{43}$ 

Upon fitting the normalized  $\eta$  to eq 6 the trap densities  $D_{it}$  at CNP for the two devices were obtained to be  $1.54 \times 10^{16}$  and  $1.91 \times 10^{16} \text{ eV}^{-1} \text{ cm}^{-3}$ , respectively, which are in good agreement with a previous study. 28 Figure 5e,f shows the normalized  $\eta$  as a function of applied gate voltage in the charge residual region for the two devices at various temperatures. A decreasing normalized  $\eta$  at both sides of the CNP at constant temperature is observed at different gate voltages within the charge residual region, indicating the progressive inaccessibility of relatively deeper trap states with increasing gate bias. On the other hand, the increase in the overall noise  $(\eta)$  with increase in temperature (either in Figure 5e,f or in Figure 5a,b) is due to the thermally activated trapping and detrapping mechanism of charge carriers from or to the percolation region with the puddles. Moreover, we can also relate the noise behavior in the temperature to n\*. Since from Figure 4a we obtained that n\* increases with temperature, we can safely conclude that the noise arising from the trapping and detrapping mechanism in the percolation region increases with n\* and vice versa. This means at higher temperatures, carriers in puddles with enough thermal energy escape into the conducting percolation region (Type-II), thereby increasing the number of available carriers to undergo trapping and detrapping and leading to higher measured electrical noise. See Figure 4c for a model representation of the puddles and conductive percolation channels. This observed phenomenon has been termed as pinning and depinning of e-h puddles. Thus, we conclude that lower flat band fluctuation noise at lower temperatures can be attributed to pinned puddles and higher noise at higher temperatures can be attributed to unpinned puddles.

Finally, the discrepancies in the noise spectral density at the residual charge region (between similar FET devices) as shown in Figure 2g,h based on Hooge's mobility fluctuations model can be interpreted consistently as shown in Figure 5e,f with a noise model based on a flat band fluctuation model (McWorter

charge fluctuation model) involving e-h puddles and percolation transport in high performance 2D-HGFETs. In order to justify the consistency between Figure 2g,h and Figure 5e,f, we discuss a correlated model as follows.

The normalized current spectral density according to the charge carrier trapping model with correlated mobility fluctuations (number and mobility fluctuations) studied bt Ghibaudo et al. <sup>59</sup> is given by

$$\frac{S_I}{I_d^2} = \left(1 \pm \alpha \mu(r) C_{ox} \frac{I_d}{g_m}\right)^2 \frac{g_m^2}{I_d^2} S_{Vfb}$$
 (8)

where  $\alpha$ , a correlation term, when finite, suggests the effect of mobility fluctuations on the measured current spectral density. On the other hand, when  $\alpha = 0$ , there is no mobility fluctuation on the measured current spectral density and in this case, the above equation can be simplified as (since  $(\alpha\mu)^2 \gg \alpha\mu$ )

$$\frac{S_{I}}{I_{d}^{2}} \frac{g_{m}^{2}}{I_{d}^{2}} S_{Vfb} + \alpha^{2} f(\mu) S_{Vfb}$$
(9)

Now one can see when  $\alpha=0$ , eq 9 essentially becomes eq 5; that is, a true McWhorter's number fluctuation model (number fluctuation only) dominates. However, when  $\alpha\neq 0$ , which is typically on the order of  $10^4$ , there exist correlated mobility fluctuations (number and mobility fluctuations). The plot for  $\alpha^2 f(\mu)$  for  $\alpha=10^4$  V s/C is shown below in similar  $V_{\rm g}-V_{\rm CNP}$  values which exhibits a "V" shape at both 80 and 295 K. From the plot, one can expect a "V" shape when  $\alpha\neq 0$ : i.e., when there is contribution from mobility fluctuations. On the other hand, when  $\alpha=0$ , the origin of noise can be explained by flat band fluctuation as explained in detail in the manuscript which shows a " $\Lambda$ " shape. This understanding is aided further in Figure S2 in the Supporting Information.

Therefore, the as-seen difference between the measured normalized current spectral density in the two SLG devices at low and high temperatures (Figure 2g,h) is explained as follows. For the "A" and "V" behaviors at 80 and 295 K, respectively, in SLG device 1 (as seen in Figure 2g), at 295 K, with high thermal activation energies, the carriers within the puddle region in graphene channel get trapped and detrapped at deeper trap levels with a high degree of fluctuations in mobility  $(\alpha \neq 0)$ , thus giving the characteristic "V" shape to power spectral density. On the other hand, at 80 K, the deep level trap states are not accessible to the channel due to less thermal activation and thereby do not create a significant effect in mobility fluctuations ( $\alpha = 0$ ). This gives a " $\Lambda$ " shape to the measured current power spectral density. SLG device 2, on the other hand, shows a "A" shape at both low and high temperatures, suggesting significantly less trapping and detrapping of carriers from the deep trap levels with reduced or no mobility fluctuation contribution to measured noise spectra. For the " $\Lambda$ " behaviors at both the temperatures in SLG device 2 (as seen in Figure 2h),  $\alpha = 0$  is maintained due to the inaccessible nature of the deep level trap states to the channel. In summary, the difference observed in different behaviors can be explained by relative contributions between the number fluctuation model and a hybrid number-mobility fluctuation model (dictated by whether  $\alpha = 0$  or  $\alpha \neq 0$ , respectively). The effect of the number fluctuation model only leads to a "A" shape, as shown in Figure 2h, whereas a hybrid contribution shows a "V" shape as shown in Figure 2g.

#### CONCLUSIONS

In conclusion, 1D contacts to 2D-HGFETs not only show high-performance transistor characteristics in the ON state of the devices but also provide a test bed for studying transport and low-frequency noise involving electron-hole puddles near the charge neutrality point. Our analysis overcomes the ambiguity on low-frequency noise trends in the charge neutrality region that is based on Hooge's mobility fluctuation model. More generally, near the charge neutrality region of single-layer graphene devices, the LFN is described by a correlated mobility number and mobility fluctuations of charge carriers. The characteristic percolation transport of the charge carriers and their low-frequency noise arising from flat band fluctuations in these devices could thus be further engineered for studying the fundamental properties of artificial materials involving atomically thin heterostructures. The high mobility and high sensitivity of the transistor channel to flat band fluctuations in these devices could thus be uniquely exploited in applications such as RF communications and precision sensing.

## ASSOCIATED CONTENT

#### **Data Availability Statement**

The data that support the findings of this study are available from the corresponding authors upon reasonable request.

# Supporting Information

The Supporting Information is available free of charge at https://pubs.acs.org/doi/10.1021/acsanm.4c00367.

Electrical transfer characteristics and correlated mobility fluctuation plot (PDF)

# AUTHOR INFORMATION

#### **Corresponding Author**

Suprem R. Das — Department of Industrial and Manufacturing Systems Engineering and Department of Electrical and Computer Engineering, Kansas State University, Manhattan, Kansas 66506, United States;
orcid.org/0000-0003-0334-7600; Email: srdas@ksu.edu

#### Authors

Aroop K. Behera – Department of Industrial and Manufacturing Systems Engineering, Kansas State University, Manhattan, Kansas 66506, United States

C. Thomas Harris — Center for Integrated Nanotechnologies, Sandia National Laboratories, Albuquerque, New Mexico 87123, United States; Sandia National Laboratories, Albuquerque, New Mexico 87185, United States

Douglas V. Pete – Center for Integrated Nanotechnologies, Sandia National Laboratories, Albuquerque, New Mexico 87123, United States; Sandia National Laboratories, Albuquerque, New Mexico 87185, United States

Christopher M. Smyth — Sandia National Laboratories, Albuquerque, New Mexico 87185, United States; orcid.org/0000-0003-4668-9555

Marta B. Muniz – Department of Sustainable Energy Technology, SINTEF, 0373 Oslo, Norway; Institut de Physique de la Matieère Complexe, Ecole Polytechnique Fèdèrale de Lausanne (EPFL), 1015 Lausanne, Switzerland

Ozhan Koybasi – Department of Smart Sensors and Microsystems, SINTEF DIGITAL, 0373 Oslo, Norway Takashi Taniguchi – Research Center for Materials Nanoarchitectonics, National Institute for Materials Science, Tsukuba 305-0044, Japan; o orcid.org/0000-0002-1467-3105

Kenji Watanabe — Research Center for Electronic and Optical Materials, National Institute for Materials Science, Tsukuba 305-0044, Japan; orcid.org/0000-0003-3701-8119

Branson D. Belle — Department of Sustainable Energy Technology, SINTEF, 0373 Oslo, Norway; ⊚ orcid.org/ 0000-0002-1211-8714

Complete contact information is available at: https://pubs.acs.org/10.1021/acsanm.4c00367

### **Author Contributions**

S.R.D. conceived the original idea and designed and supervised the project. A.K.B. performed the measurements and analysis. C.T.H. and D.V.P. helped in the measurement setup. C.M.S. performed the Raman measurements. B.D.B., O.K., and M.B.M. fabricated the devices. T.T. and K.W. provided hBN.

#### Notes

The authors declare no competing financial interest.

# ACKNOWLEDGMENTS

S.R.D. acknowledges financial support from the U.S. National Science Foundation (NSF) ECCS CAREER Grant No. 2145962. S.R.D. also acknowledges, in part, the work performed at the Center for Integrated Nanotechnologies, an Office of Science User Facility operated for the U.S. Department of Energy (DOE) Office of Science. Sandia National Laboratories is a multimission laboratory managed and operated by the National Technology and Engineering Solutions of Sandia, LLC., a wholly owned subsidiary of Honeywell International, Inc., for the U.S. Department of Energy's National Nuclear Security Administration under contract no. DE-NA0003525. This paper describes objective technical results and analysis. Any subjective views or opinions that might be expressed in the paper do not necessarily represent the views of the U.S. Department of Energy or the United States Government. B.D.B. acknowledges support by the Research Council of Norway (project nos. 250555 and 280788). The Research Council of Norway is also acknowledged for support to the Norwegian Micro- and Nano-Fabrication Facility, NorFab, project number 295864. The authors acknowledge support from JSPS KAKENHI (Grant Numbers 19H05790, 20H00354, and 21H05233). Growth of hexagonal boron nitride was supported by the JSPS KAKENHI (Grant Numbers 20H00354, 21H05233, and 23H02052) and World Premier International Research Center Initiative (WPI), MEXT, Japan.

## REFERENCES

- (1) Jiang, Z.; Zhang, Y.; Tan, Y. W.; Stormer, H. L.; Kim, P. Quantum Hall Effect in Graphene. *Solid State Commun.* **2007**, *143* (1–2), 14–19.
- (2) Morozov, S. V.; Novoselov, K. S.; Katsnelson, M. I.; Schedin, F.; Ponomarenko, L. A.; Jiang, D.; Geim, A. K. Strong Suppression of Weak Localization in Graphene. *Phys. Rev. Lett.* **2006**, *97* (1), 7–10.
- (3) Gorbachev, R. V.; Tikhonenko, F. V.; Mayorov, A. S.; Horsell, D. W.; Savchenko, A. K. Weak Localization in Bilayer Graphene. *Phys. Rev. Lett.* **2007**, 98 (17), 3–6.
- (4) Hogan, C. J.; Ostriker, J. P.; Turok, N.; Bryan, G. L.; Norman, M. L.; Coppi, P. S.; Larson, R. B.; Omukai, K.; Hernguist, L.; Abel, T.; White, S. D. M.; Jenkins, A.; Frenk, C. S.; Springel, V.; Palla, F.; Hooper, D.; Silk, J.; Widrow, L. M.; Lesgourgues, J.; Haehnelt, M. G.; Matarrese, S.; Riotto, A.; Makarov, A.; Mcdonald, P.; Trac, H.; White,

- S. D. M.; Bromm, V.; Oh, S. P.; Kitayama, T.; Hernquist, L.; Miyama, S. M.; Umemura, M.; Nishi, R. Phase-Coherent Transport in Graphene Quantum Billiards. *Science* **2007**, *317*, 1530.
- (5) Das Sarma, S.; Adam, S.; Hwang, E. H.; Rossi, E. Electronic Transport in Two-Dimensional Graphene. *Rev. Mod. Phys.* **2011**, 83 (2), 407–470.
- (6) Hwang, E. H.; Adam, S.; Sarma, S. D. Carrier Transport in Two-Dimensional Graphene Layers. *Phys. Rev. Lett.* **200**7, *98* (18), 2–5.
- (7) Geim, A. K. Graphene: Status and Prospects. Science 2009, 324, 1530-1535.
- (8) Novoselov, K. S.; Geim, A. K.; Morozov, S. V.; Jiang, D.; Zhang, Y.; Dubonos, S. V.; Grigorieva, I. V.; Firsov, A. A. Electric Field Effect in Atomically Thin Carbon Films. *Science* **2016**, *306* (5696), 666–669
- (9) Novoselov, K. S.; Geim, A. K.; Morozov, S. V.; Jiang, D.; Katsnelson, M. I.; Grigorieva, I. V.; Dubonos, S. V.; Firsov, A. A. Two-Dimensional Gas of Massless Dirac Fermions in Graphene. *Nature* **2005**, 438 (7065), 197–200.
- (10) Morozov, S. V.; Novoselov, K. S.; Katsnelson, M. I.; Schedin, F.; Elias, D. C.; Jaszczak, J. A.; Geim, A. K. Giant Intrinsic Carrier Mobilities in Graphene and Its Bilayer. *Phys. Rev. Lett.* **2008**, *100* (1), 11–14.
- (11) Castro Neto, A. H.; Guinea, F.; Peres, N. M. R.; Novoselov, K. S.; Geim, A. K. The Electronic Properties of Graphene. *Rev. Mod. Phys.* **2009**, *81* (1), 109–162.
- (12) Dutta, P.; Horn, P. M. Low-Frequency Fluctuations in Solids: If Noise. Rev. Mod. Phys. 1981, 53 (3), 497–516.
- (13) Lin, Y. M.; Avouris, P. Strong Suppression of Electrical Noise in Bilayer Graphene Nanodevices. *Nano Lett.* **2008**, 8 (8), 2119–2125.
- (14) Pal, A. N.; Ghatak, S.; Kochat, V.; Sneha, E. S.; Sampathkumar, A.; Raghavan, S.; Ghosh, A. Microscopic Mechanism of 1/f Noise in Graphene: Role of Energy Band Dispersion. *ACS Nano* **2011**, *5* (3), 2075–2081.
- (15) Kumar, C.; Kuiri, M.; Jung, J.; Das, T.; Das, A. Tunability of 1/f Noise at Multiple Dirac Cones in HBN Encapsulated Graphene Devices. *Nano Lett.* **2016**, *16* (2), 1042–1049.
- (16) Kumar, M.; Laitinen, A.; Cox, D.; Hakonen, P. J. Ultra Low 1/f Noise in Suspended Bilayer Graphene. *Appl. Phys. Lett.* **2015**, *106* (26), 263505.
- (17) Bolotin, K. I.; Sikes, K. J.; Hone, J.; Stormer, H. L.; Kim, P. Temperature-Dependent Transport in Suspended Graphene. *Phys. Rev. Lett.* **2008**, *101* (9), 5–8.
- (18) Liao, L.; Duan, X. Graphene for Radio Frequency Electronics. *Mater. Today* **2012**, *15* (7–8), 328–338.
- (19) Razavieh, A.; Singh, N.; Paul, A.; Klimeck, G.; Janes, D.; Appenzeller, J. A New Method to Achieve RF Linearity in SOI Nanowire MOSFETs. Dig. Pap. IEEE Radio Freq. Integr. Circuits Symp. 2011, 1–4.
- (20) Wang, L.; Meric, I.; Huang, P. Y.; Gao, Q.; Gao, Y.; Tran, H.; Taniguchi, T.; Watanabe, K.; Campos, L. M.; Muller, D. A.; Guo, J.; Kim, P.; Hone, J.; Shepard, K. L.; Dean, C. R. One-Dimensional Electrical Contact to a Two-Dimensional Material. *Science* (80-.). **2013**, 342 (6158), 614–617.
- (21) Mayorov, A. S.; Gorbachev, R. V.; Morozov, S. V.; Britnell, L.; Jalil, R.; Ponomarenko, L. A.; Blake, P.; Novoselov, K. S.; Watanabe, K.; Taniguchi, T.; Geim, A. K. Micrometer-Scale Ballistic Transport in Encapsulated Graphene at Room Temperature. *Nano Lett.* **2011**, *11* (6), 2396–2399.
- (22) Liu, Y.; Dong, X.; Chen, P. Biological and Chemical Sensors Based on Graphene Materials. *Chem. Soc. Rev.* **2012**, *41* (6), 2283–2307
- (23) Kang, X.; Wang, J.; Wu, H.; Aksay, I. A.; Liu, J.; Lin, Y. Glucose Oxidase-Graphene-Chitosan Modified Electrode for Direct Electrochemistry and Glucose Sensing. *Biosens. Bioelectron.* **2009**, 25 (4), 901–905.
- (24) Huang, Y.; Dong, X.; Liu, Y.; Li, L. J.; Chen, P. Graphene-Based Biosensors for Detection of Bacteria and Their Metabolic Activities. *J. Mater. Chem.* **2011**, *21* (33), 12358–12362.

- (25) Ohno, Y.; Maehashi, K.; Inoue, K.; Matsumoto, K. Label-Free Aptamer-Based Immunoglobulin Sensors Using Graphene Field-Effect Transistors. *Jpn. J. Appl. Phys.* **2011**, *50* (7), 070120.
- (26) Hooge, F. N. 1/f Noise Is No Surface Effect. Phys. Lett. A 1969, 29 (3), 139–140.
- (27) McWhorter, A. L. Semiconductor Surface Physics; Kingston, R. H., Ed.; University of Pennsylvania Press: 1957; p 207.
- (28) Kakkar, S.; Karnatak, P.; Ali Aamir, M.; Watanabe, K.; Taniguchi, T.; Ghosh, A. Optimal Architecture for Ultralow Noise Graphene Transistors at Room Temperature. *Nanoscale* **2020**, *12* (34), 17762–17768.
- (29) Liu, G.; Rumyantsev, S.; Shur, M. S.; Balandin, A. A. Origin of 1/f Noise in Graphene Multilayers: Surface vs. Volume. *Appl. Phys. Lett.* **2013**, *102* (9), 093111.
- (30) Zhang, Y.; Mendez, E. E.; Du, X. Mobility-Dependent Low-Frequency Noise in Graphene Field-Effect Transistors. *ACS Nano* **2011**, *5* (10), 8124–8130.
- (31) Xu, G.; Torres, C. M.; Zhang, Y.; Liu, F.; Song, E. B.; Wang, M.; Zhou, Y.; Zeng, C.; Wang, K. L. Effect of Spatial Charge Inhomogeneity on 1/f Noise Behavior in Graphene. *Nano Lett.* **2010**, 10 (9), 3312–3317.
- (32) Takeshita, S.; Matsuo, S.; Tanaka, T.; Nakaharai, S.; Tsukagoshi, K.; Moriyama, T.; Ono, T.; Arakawa, T.; Kobayashi, K. Anomalous Behavior of 1/f Noise in Graphene near the Charge Neutrality Point. *Appl. Phys. Lett.* **2016**, *108* (10), 103106.
- (33) Stolyarov, M. A.; Liu, G.; Rumyantsev, S. L.; Shur, M.; Balandin, A. A. Suppression of 1/ f Noise in near-Ballistic h -BN-Graphene- h- BN Heterostructure Field-Effect Transistors. *Appl. Phys. Lett.* **2015**, *107* (2), 023106.
- (34) Kayyalha, M.; Chen, Y. P. Observation of Reduced 1/f Noise in Graphene Field Effect Transistors on Boron Nitride Substrates. *Appl. Phys. Lett.* **2015**, *107* (11), 10–14.
- (35) Li, X.; Lu, X.; Li, T.; Yang, W.; Fang, J.; Zhang, G.; Wu, Y. Noise in Graphene Superlattices Grown on Hexagonal Boron Nitride. *ACS Nano* **2015**, 9 (11), 11382–11388.
- (36) Karnatak, P.; Sai, T. P.; Goswami, S.; Ghatak, S.; Kaushal, S.; Ghosh, A. Current Crowding Mediated Large Contact Noise in Graphene Field-Effect Transistors. *Nat. Commun.* **2016**, *7*, 1–8.
- (37) Chen, J. H.; Jang, C.; Xiao, S.; Ishigami, M.; Fuhrer, M. S. Intrinsic and Extrinsic Performance Limits of Graphene Devices on SiO 2. *Nat. Nanotechnol.* **2008**, 3 (4), 206–209.
- (38) Hwang, E. H.; Das Sarma, S. Acoustic Phonon Scattering Limited Carrier Mobility in Two-Dimensional Extrinsic Graphene. *Phys. Rev. B Condens. Matter Mater. Phys.* **2008**, 77 (11), 115449.
- (39) Sarkar, S.; Amin, K. R.; Modak, R.; Singh, A.; Mukerjee, S.; Bid, A. Role of Different Scattering Mechanisms on the Temperature Dependence of Transport in Graphene. *Sci. Rep.* **2015**, *5*, 1–10.
- (40) Chen, J. H.; Jang, C.; Adam, S.; Fuhrer, M. S.; Williams, E. D.; Ishigami, M. Charged-Impurity Scattering in Graphene. *Nat. Phys.* **2008**, *4* (5), 377–381.
- (41) Nagashio, K.; Nishimura, T.; Kita, K.; Toriumi, A. Contact Resistivity and Current Flow Path at Metal/Graphene Contact. *Appl. Phys. Lett.* **2010**, *97* (14), 8–11.
- (42) Dean, C. R.; Young, A. F.; Meric, I.; Lee, C.; Wang, L.; Sorgenfrei, S.; Watanabe, K.; Taniguchi, T.; Kim, P.; Shepard, K. L.; Hone, J. Boron Nitride Substrates for High-Quality Graphene Electronics. *Nat. Nanotechnol.* **2010**, 5 (10), 722–726.
- (43) Behera, A. K.; Harris, C. T.; Pete, D. V.; Delker, C. J.; Vullum, P. E.; Muniz, M. B.; Koybasi, O.; Taniguchi, T.; Watanabe, K.; Belle, B. D.; Das, S. R. High-Performance and Ultralow-Noise Two-Dimensional Heterostructure Field-Effect Transistors with One-Dimensional Electrical Contacts. ACS Appl. Electron. Mater. 2021, 3, 4126.
- (44) Rossi, E.; Adam, S.; Das Sarma, S. Effective Medium Theory for Disordered Two-Dimensional Graphene. *Phys. Rev. B Condens. Matter Mater. Phys.* **2009**, 79 (24), 1–7.
- (45) Rossi, E.; Das Sarma, S. Ground State of Graphene in the Presence of Random Charged Impurities. *Phys. Rev. Lett.* **2008**, *101* (16), 8–11.

- (46) Martin, J.; Akerman, N.; Ulbricht, G.; Lohmann, T.; Smet, J. H.; Von Klitzing, K.; Yacoby, A. Observation of Electron-Hole Puddles in Graphene Using a Scanning Single-Electron Transistor. *Nat. Phys.* **2008**, *4* (2), 144–148.
- (47) Rutter, G. M.; Jung, S.; Klimov, N. N.; Newell, D. B.; Zhitenev, N. B.; Stroscio, J. A. Microscopic Polarization in Bilayer Graphene. *Nat. Phys.* **2011**, *7* (8), 649–655.
- (48) Adam, S.; Jung, S.; Klimov, N. N.; Zhitenev, N. B.; Stroscio, J. A.; Stiles, M. D. Mechanism for Puddle Formation in Graphene. *Phys. Rev. B Condens. Matter Mater. Phys.* **2011**, 84 (23), 1–7.
- (49) Adam, S.; Jung, S.; Klimov, N. N.; Zhitenev, N. B.; Stroscio, J. A.; Stiles, M. D. Mechanism for Puddle Formation in Graphene. *Phys. Rev. B Condens. Matter Mater. Phys.* **2011**, 84 (23), 1–6.
- (50) Castellanos-Gomez, A.; Buscema, M.; Molenaar, R.; Singh, V.; Janssen, L.; Van Der Zant, H. S. J.; Steele, G. A. Deterministic Transfer of Two-Dimensional Materials by All-Dry Viscoelastic Stamping. 2D Mater. **2014**, *1* (1), 011002.
- (51) Gorbachev, R. V.; Riaz, I.; Nair, R. R.; Jalil, R.; Britnell, L.; Belle, B. D.; Hill, E. W.; Novoselov, K. S.; Watanabe, K.; Taniguchi, T.; Geim, A. K.; Blake, P. Hunting for Monolayer Boron Nitride: Optical and Raman Signatures. *Small* **2011**, *7* (4), 465–468.
- (52) Tan, Y. W.; Zhang, Y.; Bolotin, K.; Zhao, Y.; Adam, S.; Hwang, E. H.; Das Sarma, S.; Stormer, H. L.; Kim, P. Measurement of Scattering Rate and Minimum Conductivity in Graphene. *Phys. Rev. Lett.* **2007**, *99* (24), 10–13.
- (53) Adam, S.; Hwang, E. H.; Galitski, V. M.; Das Sarma, S. A Self-Consistent Theory for Graphene Transport. *Proc. Natl. Acad. Sci. U. S. A.* **2007**, *104* (47), 18392–18397.
- (54) Gibertini, M.; Tomadin, A.; Guinea, F.; Katsnelson, M. I.; Polini, M. Electron-Hole Puddles in the Absence of Charged Impurities. *Phys. Rev. B Condens. Matter Mater. Phys.* **2012**, 85 (20), 1–5.
- (55) Yankowitz, M.; Xue, J.; Leroy, B. J. Graphene on Hexagonal Boron Nitride. J. Phys.: Condens. Matter 2014, 26 (30), 303201.
- (56) Xue, J.; Sanchez-Yamagishi, J.; Bulmash, D.; Jacquod, P.; Deshpande, A.; Watanabe, K.; Taniguchi, T.; Jarillo-Herrero, P.; Leroy, B. J. Scanning Tunnelling Microscopy and Spectroscopy of Ultra-Flat Graphene on Hexagonal Boron Nitride. *Nat. Mater.* **2011**, *10* (4), 282–285.
- (57) Li, Q.; Hwang, E. H.; Das Sarma, S. Disorder-Induced Temperature-Dependent Transport in Graphene: Puddles, Impurities, Activation, and Diffusion. *Phys. Rev. B Condens. Matter Mater. Phys.* **2011**, *84* (11), 115442.
- (58) Vandamme, L. K. J. How Useful Is Hooge's Empirical Relation. 2013 22nd Int. Conf. Noise Fluctuations, ICNF 2013, 2013.
- (59) Ghibaudo, G.; Roux, O.; Nguyen-Duc, C.; Balestra, F.; Brini, J. Improved Analysis of Low Frequency Noise in Field-Effect MOS Transistors. *Phys. Status Solidi* **1991**, *124* (2), 571–581.
- (60) Ghatak, S.; Mukherjee, S.; Jain, M.; Sarma, D. D.; Ghosh, A. Microscopic Origin of Low Frequency Noise in MoS2 Field-Effect Transistors. *APL Mater.* **2014**, *2* (9), 092515.